now published as :C. Chiccoli, P. Pasini, G. Skacej, C. Zannoni, S. Zumer, Nematics with dispersed polymer fibrils: A Monte Carlo study of the external field-induced switching, Phys. Rev. E, Rapid Comm., 67, 010701.1-4 (2003).

Nematics with dispersed polymer fibrils: A Monte Carlo study of the external field-induced switching

C. Chiccoli[1], P. Pasini[1], G. Skačej[2], C. Zannoni[3], and S. Žumer[2]
[1] *INFN, Sezione di Bologna, Via Irnerio 46, I-40126 Bologna, Italy*
[2] *Oddelek za fiziko, Univerza v Ljubljani, Jadranska 19, SI-1000 Ljubljana, Slovenia*
[3] *Dip. di Chimica Fisica ed Inorganica and INSTM, Università, Viale Risorgimento 4, I-40136 Bologna, Italy*
(May 24, 2002)

We present a Monte Carlo study of molecular ordering in nematics with dispersed regular and random arrays of straight and distorted polymer fibrils. We focus on the collective molecular reorientation — the switching — resulting from the competing aligning effects of fibrils and of a progressively applied transversal electric field, and identify stuctural Fréedericksz and saturation transitions. The role of fiber topography in the switching behavior is monitored by simulating electric capacitance: slightly distorted fibrils are shown to give a sharper switching.

PACS number(s): 61.30.Cz, 61.30.Gd

While simple nematic liquid crystals (LC) are now well understood, nano and mesoscale composites where LC interact with random or regular perturbers [1–3] offer fascinating examples of complex systems, challenging both from the technological and fundamental point of view. Such perturbers consist, e.g., of thin (even nanometric) polymer fibers obtained by polymerization of monomers dissolved in LC that can either memorize the order of the host LC phase [3], or follow a regular pattern as defined in a lithographic formation process [4]. The fiber topography depends sensitively on the polymerization conditions, such as temperature, curing light wavelength and intensity, or monomer solubility [5]. Because of their high surface-to-volume ratio the polymer fibrils influence orientational ordering of the surrounding liquid crystal even at low polymer concentrations [3,6–8]. The actual ordering is affected by the competition between effects of the fiber network (anchoring), temperature, and external fields. Apart from exhibiting a variety of interesting confinement-related phenomena, such composite materials are promising also for the construction of electrooptical devices, based on the "switching" phenomenon. This consists of a reorganization of the nematic director — initially aligned by the polymer network — by applying an external electric field producing changes in electric capacitance, optical transmission, light scattering, etc [3,6–8]. Thus studies of formation and properties of liquid crystal-dispersed network systems (LCDNS) are very timely, also for the next generation of LC displays [4,6]. In the past there have been several studies devoted to LCDNS, both experimental and theoretical [6–8], but so far the effect of such complex confinement was described only phenomenologically in terms of an effective field [6], while there have been virtually no investigations at the microscopic level [9]. In this Letter we investigate the field-induced changes of molecular ordering in LCDNS by means of Monte Carlo (MC) simulations, starting from a simple pairwise potential and giving great emphasis to the role of polymer network topography.

Our simulations are based on the Lebwohl-Lasher (LL) model [10] in which uniaxial nematic molecules (or close-packed clusters containing up to 10^2 molecules [11]) are represented by unit vectors ("particles") $\mathbf{u}_i$. The LL model, despite having particles fixed onto sites of a cubic lattice (with spacing a, 1 nm $\lesssim a \lesssim$ 5 nm), reproduces the orientational behavior of nematics sufficiently well [11]. We model the effect of an external field by adding a quadratic contribution to the LL Hamiltonian [11]. The total interaction energy for a system of N particles is then given by

$$U_N = -\sum_{\langle i<j\rangle} \epsilon_{ij}\, P_2(\mathbf{u}_i \cdot \mathbf{u}_j) - \epsilon\eta \sum_{i=1}^{N} P_2(\mathbf{f} \cdot \mathbf{u}_i), \qquad (1)$$

where $P_2(x) = \frac{1}{2}(3x^2 - 1)$, $\mathbf{f}$ stands for a unit vector oriented along the external field $\mathbf{E}$ ($\mathbf{E} = E\mathbf{f}$), and ϵ_{ij} is a positive constant, nonzero only for nearest-neighbor particles: ϵ for nematic-nematic interactions and $w\epsilon$ for nematic-polymer interactions (also included in the first sum). Moreover, dimensionless $\eta \propto E^2$ gives the strength of the coupling with the field. In practice, $\mathbf{E}$ could be an electric or magnetic field [12]. For simplicity, $\mathbf{E}$ was assumed homogeneous throughout the sample despite the (possibly strong) inhomogeneity of the nematic.

As a first step towards modeling the topography of the polymer network, we consider a single straight cylindrical fiber oriented along the z-axis by defining a "jagged" cylinder comprising all the particles lying closer than R (the fiber radius) from the center of the xy-section [9]. Here the x, y, and z-axes coincide with the edges of the cubic lattice. Particle orientations in the fiber surface layer ("ghosts") were fixed in accordance with the desired surface anchoring (here chosen parallel to the fiber direction, z-axis) and the corresponding dimensionless anchoring strength was introduced above as $w > 0$. The field was applied along the y-axis, thereby producing a conflict with the aligning tendency of the polymer network. Periodic boundary conditions were assumed at outer simulation box boundaries, hence such a set-up ("sample A")

may be regarded as a regular array of straight and parallel fibers.

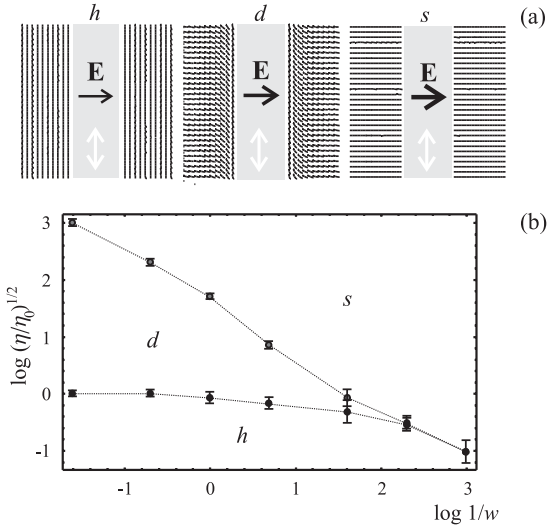

FIG. 1. Structural transitions in sample A. (a) Director fields $\mathbf{n}(\mathbf{r})$ (yz-cross sections) for the three possible structures (calculated for $\eta = 0.005$, 0.05, and 0.5). $\mathbf{n}(\mathbf{r})$ in each point was calculated by diagonalizing the MC cycle-averaged local ordering matrix $\mathsf{Q} = \frac{1}{2}(3\langle \mathbf{u}_i \otimes \mathbf{u}_i \rangle - \mathsf{I})$ and identifying the eigenvector corresponding to the eigenvalue with the largest absolute value. (b) The structural phase diagram; η_0 denotes the Fréedericksz threshold for $w = 5$ (strong anchoring).

We introduce notation in analogy with the switching in a nematic slab where surface anchoring is strong and planar, and a field is applied along the slab normal. In weak fields the equilibrium director ($\mathbf{n}$) configuration is homogeneous with $\mathbf{n} \perp \mathbf{f}$ ("h-structure"). Increasing the field strength, once the Fréedericksz threshold $E_F = \sqrt{k/\epsilon_a \epsilon_0}(\pi/\delta)$ is reached, a continuous transition to a deformed structure is observed ("d-structure"). Here k denotes the effective Frank elastic constant, δ the sample thickness, $\epsilon_a = \epsilon_{||} - \epsilon_\perp$ the anisotropy of the dielectric constant ($||$ and $\perp$ referring to $\mathbf{n}$), and ϵ_0 its vacuum value. For finite anchoring strengths w the threshold E_F is somewhat reduced [13]. Increasing E even further, for finite w the field overwhelms the anchoring and a second, also continuous "saturation" transition takes place. Above this second threshold E_s — showing a more significant w-dependence than E_F — nematic molecules are aligned uniformly along the field, with $\mathbf{n}||\mathbf{f}$ ("s-structure"). Both thresholds, E_F and E_s, have been derived numerically for an arbitrary w in slab geometry, allowing for the construction of a stability phase diagram for the three possible structures [13]. In case of weak anchoring or in a very thin nematic slab with $k/w \gg \delta$, the thresholds E_F and E_s attain similar values, whereby the stability region for the d-structure becomes extremely narrow [13]. There is, however, no triple point in the diagram.

We observe a similar switching behavior also in an array of polymer fibers, sample A. The yz-cross sections of director profiles calculated for each of the three structure types are shown in Fig. 1 (a) and the structural phase diagram in Fig. 1 (b). Note that for the d-structure the nematic is bent in the yz-plane, while it is twisted in the xz-plane, as opposed to the slab case where the twist deformation is absent. The intermolecular potential (1), however, is spatially isotropic and corresponds to the one-constant approximation in the Frank elastic description, making thus no distinction in energy for the different deformation modes and causing the switching behavior to be qualitatively close to that observed in slab geometry.

Constructing the diagram, the simulation box size was set to $30 \times 30 \times 30$ particles, which for the chosen fiber radius ($R/a = 5$) amounts to 24600 nematic and 840 ghost particles in total. Then, for each anchoring strength w, the zero-field simulation ($\eta = 0$) started from a completely random orientational configuration, and the Metropolis scheme [14] was employed to update particle orientations [11]. Once the system was equilibrated (after at least 1.2×10^5 MC cycles), a set of further 1.2×10^5 successive cycles was used to calculate relevant observables. In cases with an external field applied ($\eta > 0$), the simulation started from the configuration equilibrated at the next lowest field strength E, thus performing a "scan" increasing E (and η). For checking, a similar scan was performed also decreasing η. The order parameter sensitive to field-induced orientational changes was defined as $\langle P_2^f \rangle = \langle \frac{1}{2}[3(\mathbf{u}_i \cdot \mathbf{f})^2 - 1] \rangle$, where the brackets $\langle ... \rangle$ represent an average over nematic particles and over MC cycles. Then, the η value yielding the maximum σ^f — the variance of $\langle P_2^f \rangle$ related to collective molecular fluctuations — can be used as a reliable enough estimate for the structural transition threshold. Note, however, that if the average $\langle ... \rangle$ above is taken over all nematic particles, monitoring σ^f one can detect only the Fréedericksz transition involving a large portion of nematic material. On the other hand, to detect the saturation transition affecting only a few particles near the fiber surface, the average $\langle ... \rangle$ is to be calculated exclusively over particles in a thin layer surrounding the fiber (of thickness $\sim a$).

The phase diagram [Fig. 1 (b)] was derived for $T^* = k_B T/\epsilon = 1.0$ (recall that the bulk nematic-isotropic transition is observed at $T^*_{NI} = 1.1232$ [11]) and shows stability regions for the h, d, and s director structures. In weak fields one can always find the undistorted h-structure, while in strong enough fields the saturated s-structure is always seen. The deformed d-structure appears at intermediate field strengths, but like in slab geometry its stability region gets narrower upon decreasing w. Due to the low accuracy of threshold estimates for small w we cannot clearly confirm the absence of the triple point in the diagram. Further, both transitions seem to be continuous: no systematic hysteresis could be detected in external field scans.

In Fig. 1 (b) the Fréedericksz threshold ($h \leftrightarrow d$ line; $\eta_F = 0.0085 \pm 0.0015$ for $w = 1$) indeed decreases with decreasing w, while the saturation threshold ($d \leftrightarrow s$ line;

$\eta_s = 0.30 \pm 0.015$ for $w = 1$) shows an even more significant w-dependence, approaching $\sqrt{\eta_s} \propto w$ for large w. Similarly as in slab geometry, the position of the $h \leftrightarrow d$ line is expected to strongly depend on the effective fiber-to-fiber distance d_* — with increasing d_* it should move towards lower critical field strengths — while the position of the $d \leftrightarrow s$ line for large enough w should be almost insensitive to changing d_*. One can check these statements by exploring transitions in a network consisting of somewhat thinner fibers: setting $R/a = 3$ and considering a $18 \times 18 \times 18$ sample with a single fiber approximately maintains the polymer concentration, but decreases the fiber-to-fiber distance from $d_* = 20a$ to $d'_* = 12a$. Having fixed $w = 1$ corresponding to rather strong anchoring with a microscopic extrapolation length k/w (of the order of $\sim a$), the Fréedericksz and saturation thresholds are now found to be $\eta'_F = 0.025 \pm 0.005$ and $\eta'_s = 0.30 \pm 0.03$, respectively. While η_s remained almost unaltered, η_F changed quite significantly, yielding $\sqrt{\eta_F/\eta'_F} \approx 0.58$. This compares well to $d'_*/d_* = 0.6$, which is in agreement with $\sqrt{\eta_F} \propto 1/d_*$ predicted for slab geometry in the strong anchoring limit. Finally, the temperature dependence (in principle) enters the thresholds via k, w, and ϵ_a (all decrease with increasing T^*), which will be discussed elsewhere. Preliminary results, however, indicate no dramatic changes in the phase diagram with changing T^*.

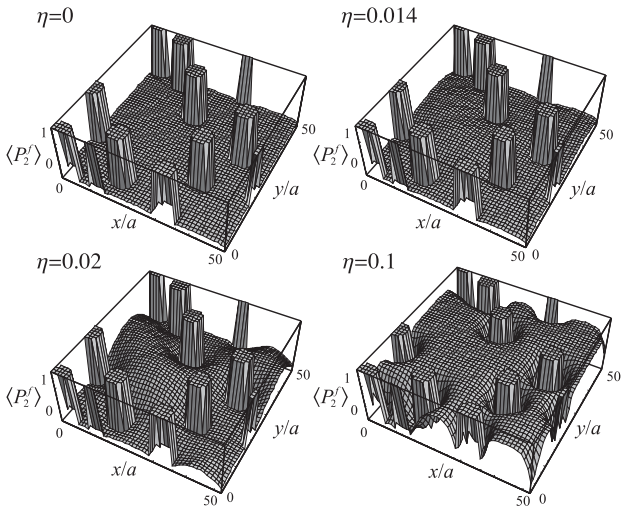

FIG. 2. Array of several straight fibers (sample B): $\langle P_2^f \rangle(\mathbf{r})$ order parameter (xy-cross section) for different field strengths (proportional to $\sqrt{\eta}$). The "columns" represent the fibers.

Although regular arrays of fibers are currently used [4], a polymer network can be much more complex [7,8]. In particular, the interfiber distance distribution is expected to play an important role in switching studies. Therefore, to increase the topographical complexity of the fiber network, we began by modeling a sample with an irregular array of fibers still straight and parallel (directed along the z-axis), yet distributed randomly within the xy-plane ("sample B"). Increasing the sample size to $50 \times 50 \times 50$ particles and including 8 fibers with $R/a = 3$ and anchoring along the z-axis ($w = 1$) again roughly maintains the polymer concentration ($\approx 9\%$). This choice hence covers linear length scales of up to ~ 0.25 μm. Again, the external field was applied along the y-axis.

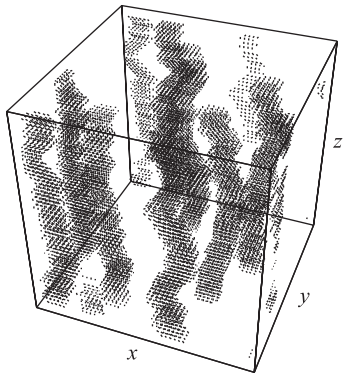

FIG. 3. Sample C with several distorted fibers: ghost particles fixing the network topography.

Fig. 2 shows the evolution of $\langle P_2^f \rangle$ averaged over MC cycles for each particle within a given xy-cross section. For $\eta \lesssim 0.013$ one finds $\langle P_2^f \rangle(\mathbf{r})$ negative and almost constant — apart from slight variations close to the fibers attributed to enhanced nematic ordering — showing that particles are still aligned along the z-axis and that the Fréedericksz threshold has not been exceeded yet. For $\eta \approx 0.013$ — still below the sample A threshold for $R/a = 3$ — in polymer-poor regions where the interfiber distance is above average the particle reorientation along $\mathbf{f}$ is initiated and $\langle P_2^f \rangle$ increases, becoming even positive. As the field strength is increased even further, the parallel-to-fiber alignment persists only very near to the fibers (as in polymer-rich regions; see Fig. 2 for $\eta = 0.1$, in the left corner). Finally, for extremely strong fields — far above the saturation transition (e.g., at $\eta = 1$) — all molecules are aligned along the field direction and, in addition, the bulk degree of nematic order is enhanced. The opposite holds for the fiber vicinity: the degree of order drops below the bulk value due to the conflicting effects of the fibers and external field. Note that unlike to the regular sample A the switching evolved into a rather gradual process in sample B.

Finally, dropping the assumption that the fibers be straight and parallel, we considered a system of distorted fibers — Fig. 3, "sample C". Again, the average fiber direction was taken along the z-axis. Then each of the fibers (with uniform cross section, $R/a = 3$) was generated by performing a biased random walk: while progressing along the z-direction, random deviations within the xy-plane were performed with a given probability regulating the fiber curvature. Doing this, care was taken to meet the periodic boundary conditions along the z-axis. Moreover, everywhere the anchoring easy axis was assumed parallel to the local fiber direction, with $w = 1$. Simulating switching in sample C, the external field was again applied along the y-axis. Despite fiber curvature, in absence of external fields ($\eta = 0$) the net molecular orientation is still well-defined (along the z-axis), except for the fiber vicinity where it is affected by the local anchoring.

For the switching in a symmetry-lacking sample it is instructive to explore simulation-predicted experimental observables, rather than study specific order parameter maps. One of the suitable tools for the monitoring of switching are electric capacitance measurements [8]. They rely on the orientational anisotropy of the molecular dielectric constant, leading to observable changes in sample capacitance for any major molecular reorientation. These changes will be monitored in the following, along with a detailed comparison of samples A, B, and C. Simulating capacitance, it was assumed that it is measured along the y-axis, i.e., between the plates used to apply the aligning external field, and that also the probing local electric field is directed along $\mathbf{f}$ everywhere in the sample. In absence of free ions and provided, moreover, that elastic deformations within the xz-plane are weak, the effective static capacitance for a $M \times M \times M$ sample can be calculated as [8]

$$C_y = \epsilon_0 \sum_{k=1}^{M} \sum_{l=1}^{M} \left(\sum_{m=1}^{M} \frac{1}{\epsilon(k,l,m)} \right)^{-1}, \qquad (2)$$

where the indices k, l, and m run along the x, z, and y coordinates, respectively. Here we consider that each group of molecules represented by the vector $\mathbf{u}_i$ and located at (k,l,m) is endowed with a local dielectric constant $\epsilon(k,l,m) = \epsilon_\perp + (\epsilon_{||} - \epsilon_\perp)(\mathbf{u}_i \cdot \mathbf{f})^2$.

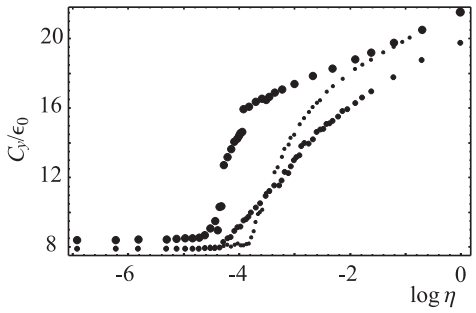

FIG. 4. Switching in LCDNS systems, as monitored via simulated electric capacitance: sample A (small dots), sample B (medium-sized dots) and sample C (large dots).

The calculations were performed for $\epsilon_{||} = 29.8$ and $\epsilon_\perp = 6.1$, assuming as in Ref. [8] the same dielectric anisotropy for the polymer network. The C_y versus η characteristics for three samples (A, B, and C) with $R/a = 3$ and same polymer concentration ($\approx 9\%$), but different network topography, is shown in Fig. 4. In Fréedericksz-like geometry where the external field is strictly perpendicular to fibers (samples A and B), the orientational transition happens abruptly at a well-defined threshold (η_A and η_B, respectively, with $\eta_A > \eta_B$). In sample C network irregularities further decrease the switching threshold (η_C; not well-defined anymore), yet keep the reorientational process relatively sudden. The thresholds for the three samples can from Fig. 4 be identified as $\eta_A = 0.022 \pm 0.001$, $\eta_B = 0.013 \pm 0.001$, and $\eta_C = 0.010 \pm 0.002$, with $\eta_C < \eta_B < \eta_A$, as expected. Note that the $C_y(\eta)$ curve is most gradual for sample B because molecules in polymer-rich sample regions refuse to switch unless the field is extremely strong. Further, the increase of C_y for large η is to be attributed to enhanced nematic order rather than to particle reorientation.

In summary, we have shown using computer simulations that — contrary to naïve intuition — external field-driven switching in a system of polymer fibers dispersed in nematics is rather sudden even in samples with a fairly disordered fiber arrangement (both positionally and orientationally), and that it appears at a lower threshold, if compared with more regular samples with same polymer concentration. These conclusions were drawn by monitoring the simulated electric capacitance, starting from the simulation data. Moreover, for a regular array of straight and parallel fibers we have simulated a stability phase diagram for possible director structures, indicating a behavior equivalent to that observed in a nematic slab. Fiber arrays with controlled disorder could probably be prepared by suitably perturbing the excitation light in the polymerization [4] and our predictions could then be tested.

G. S. acknowledges the support by CINECA through the MINOS Programme. C. Z. thanks the University of Bologna, CNR and MIUR-PRIN for support. S. Ž. is grateful to the Slovenian Office of Science (Programmes No. P0-0503-1554 and 0524-0106) and the EU (Project SILC TMR ERBFMRX-CT98-0209).

[1] T. Bellini *et al.*, Phys. Rev. Lett. **69**, 788 (1992).
[2] V. G. Nazarenko *et al.*, Phys. Rev. Lett. **87**, 075504 (2001).

[3] G. P. Crawford and S. Žumer, *Liquid Crystals in Complex Geometries Formed by Polymer and Porous Networks* (Taylor and Francis, London 1996).
[4] R. Penterman *et al.*, Nature **417**, 55 (2002).
[5] I. Dierking *et al.*, Appl. Phys. Lett. **71**, 2454 (1997); Liq. Cryst. **24**, 397 (1998); Liq. Cryst. **24**, 387 (1998).
[6] M. J. Escuti *et al.*, Appl. Phys. Lett. **75**, 3264 (1999).
[7] Y. K. Fung *et al.*, Phys. Rev. E **55**, 1637 (1997).
[8] R.-Q. Ma and D.-K. Yang, Phys. Rev. E **61**, 1567 (2000).
[9] C. Chiccoli *et al.*, Phys. Rev. E **65**, 051703 (2002).
[10] P. A. Lebwohl and G. Lasher, Phys. Rev. A **6**, 426 (1972).
[11] P. Pasini and C. Zannoni, eds., *Advances in the Computer Simulations of Liquid Crystals* (Kluwer, Dordrecht 2000).
[12] E. Berggren *et al.*, Phys. Rev. E **49**, 614 (1994).
[13] J. Nehring *et al.*, J. Appl. Phys. **47**, 850 (1976).
[14] N. Metropolis *et al.*, J. Chem. Phys. **21**, 1087 (1953).